Modeling of Hyperelastic Water-Skipping Spheres using Abaqus/Explicit

Michael A. Jandron[1], Randy C. Hurd[2], Jesse L. Belden[1], Allan F. Bower[3], William Fennell[1] and Tadd T. Truscott[2]

[1]Naval Undersea Warfare Center, Newport, RI

[2]Dept. of Mechanical Engineering, Brigham Young University, Provo, UT

[3]School of Engineering, Brown University, Providence, RI

***Abstract**: This research seeks to model and elucidate the physics of water impact of elastomeric spheres, including the mechanisms by which severe deformations enable spheres to skip off the free water surface. The interplay between solid mechanics and fluid mechanics, or fluid-structure interaction, is extremely rich and complicated for this physical phenomenon. This research and knowledge could lead to exciting applications such as the novelty products from Waboba Inc. Numerical simulations are performed in Abaqus/Explicit of a highly-compliant elastomeric sphere impacting a free surface of water using a Coupled Euler-Lagrangian (CEL) approach. Here, the spheres are modeled using a non-linear hyperelastic constitutive law in a Lagrangian frame and the fluid flow is determined by numerically solving the Navier-Stokes equations in an Eulerian frame. In addition, rate dependent effects of the elastomer are included using a linear viscoelasticity model calibrated from dynamic experiments. For validation, the simulations are compared to experiments. The testing utilizes multiple high-speed cameras which capture the sphere kinematics and vibrational modes of deformation in addition to collision timescales and details of the shape of the cavity formed in the liquid. The influence of various conditions - such as mesh convergence and contact sensitivity - on simulation results will be discussed. In addition, several benchmarking results will be shown and physical insight will be drawn from the models to help better understand the basic physics of water-skipping spheres.*

***Keywords**: Fluid-Structure Interaction, Hyperelasticity, Viscoelasticity, Constitutive Model, Rubber, Elastomer, Skipping Sphere, Coupled Euler-Lagrangian, Dynamic Mechanical Analysis, Prony Series, Stress Relaxation, High Speed Photography, Dynamic Explicit, Dragon-Skin Silicone, neo-Hookean, Ogden.*

1. Introduction

The phenomena of ricochet from a water surface is an interesting case of fluid-structure interaction characterized by large impact forces and rapid vertical accelerations as the object launched at the surface skips back into the air. The seminal water-skipping act is, arguably, stone skipping. Motivated by a desire to break the world record for most stone skips on water, researchers studied the physics of skipping stones and determined the optimal attack angle should be about 20° (Clanet, 2004, Rosellini, 2005). Several applications have motivated basic research into the physics of oblique water impact of other canonical shapes as well. A significant amount of work also exists pertaining to water entry of rigid projectiles at shallow angles to the surface (e.g., Miloh, 1991, Truscott, 2009, May, 1975). Beyond just stones, spheres can also be skipped on water (Johnson, 1975). To achieve skipping with rigid spheres the impact angle must be less than a critical angle given by

$$\theta = 18/\sqrt{\gamma} \tag{1}$$

where γ is the specific gravity of the sphere material. Equation 1 gives the impression that spheres with a specific gravity equal to unity will not skip at angles greater than 18º. However, we ask what happens if the sphere is deformable? Belden (Belden, 2012) makes the observation that highly deformable spheres skip at angles much greater than this. In fact, several commercial products exist with this intent in mind; an example is Waboba® , which makes aquatic toys. Figure 1 shows one such ball thrown at the surface of a lake. The sphere skips an astonishing 23 times before landing on the opposite shore of the lake approximately 46 m away (Figure 1(h)), begging the question: what are the physical mechanisms that allow this ball to skip so well on water?

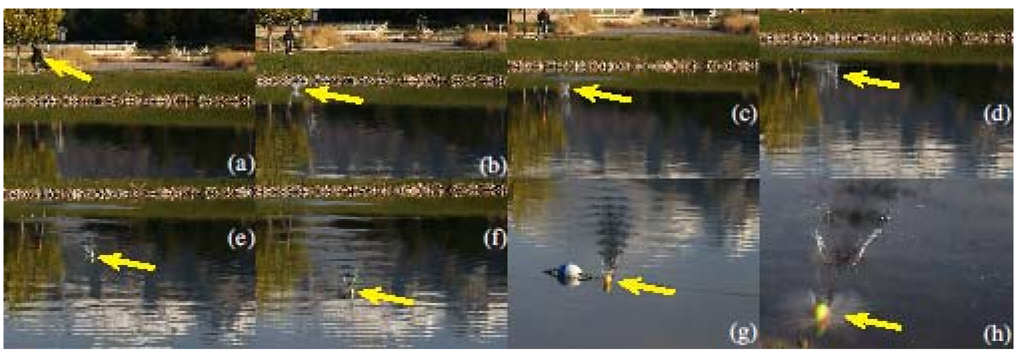

Figure 1. Sequence of highly deformable Waboba® ball skipping on the surface of a lake. (a) shows a person winding up to throw the ball and (b)-(d) show the first 3 skips, respectively. (e)-(g) show skipping downrange, which occurs at closer spacings, and (h) shows the 23rd skip, just before the ball reaches the opposite shore about 46 m away.

Belden et al. hypothesized that the ability of these elastomeric spheres to skip at conditions which violate the rigid sphere case in Equation 1 are due to the elastic "pancaking" effect of the sphere upon impact with the free water surface. The increased surface are and force coefficient result in a larger hydrodynamic force that lifts the sphere off the water. The elastomer enables this effect by converting a portion of the kinetic energy in the sphere into strain energy. This strain energy is then returned to kinetic energy which enables the sphere to rebound from the surface. A portion of the energy of the sphere is also transmitted to the fluid, and thus the optimal case for skipping is one where the maximum amount of energy is retained in the sphere; i.e. kinetic energy is converted to strain energy and then restored entirely to kinetic energy. Minimization of the energy loss by hysteretic damping and energy loss into the fluid are thus important characteristics which enable the sphere to gracefully skip multiple times. The inclusion of deformation into the water skipping problem also introduces a second fundamental timescale: a deformation time. The success of skipping is shown to depend on the interplay between the collision time and the deformation time. The collision time is the time that the sphere is in contact with the water, and the deformation time is the time it takes for an elastic wave to propagate through the elastomer and impact the fluid cavity wall. As will be shown, the competition between these two timescales plays a role in the amount of energy lost to the fluid.

In this paper we model the dynamic water skipping of elastomeric spheres using Abaqus/Explicit. Custom made elastomeric spheres that skip on water are constructed for benchmarking experiments. Extensive material testing and modeling is performed to garner accurate material response properties – including hyperelastic and viscoelastic behavior – or incorporation into the Abaqus/CAE model. The choice of elastomer and material testing and modeling are described herein. Several considerations for the Abaqus/CAE model, such as mesh size and boundary conditions, are explored. The numerical water-skipping model is implemented for several different cases of water impact velocity and results are qualitatively and quantitatively compared to the experiments.

2. Choice of Elastomer

In order to control the material properties for the spheres used in experimentation, spheres were custom made. This provided control of the material choice, and also the ability to mold experimental specimens, such as the ASTM dogbone. Deformable spheres were fabricated using Dragon Skin® series silicone rubber from the elastomer supplier Smooth-on. This material features the nominal properties by the manufacturer as shown in Table 1. This particular platinum cure silicone rubber was made by mixing parts A and B, adding a particular ratio of silicone thinner to reduce polymer cross-linking density and pouring the resulting mixture into a plastic spherical mold to cure. The mixture ratios of parts A and B were measured by mass using a laboratory scale. For the present study, no thinner was added. Equal parts A and B were mixed by hand in a plastic polyethylene cylinder. After batches had been thoroughly mixed by hand they were placed in a small vacuum chamber for 2-4 minutes to remove entrained air produced by the mixing process. The contents were then poured into plastic molds to form both spheres and thin sample sheets and allowed to cure overnight. All specimens were allowed to cure naturally and curing was not accelerated with heat treatment.

Table 1. Nominal mechanical properties for Dragon Skin® 10 Slow.

Elongation at Break [%]	Mixed Viscosity [Pa*s]	Pot Life [Min]	Shore A Hardness	Tear Strength [N/mm]	Specific Gravity, γ
1000%	23	45	10	17.86	1.073

3. Modeling Approach using Abaqus/Explicit

Abaqus/Explicit is employed to model the fluid-structure interaction using a Coupled Euler-Lagrangian (CEL) formulation. The attractiveness of this method is that the fluid is modeled in an Eulerian frame while the sphere can still be modeled in a Lagrangian frame as is typical for solid mechanics applications. Specifically, in CEL, the governing equation of the solid uses the conservation of momentum, while the governing equation for the fluid uses a general form of Navier-Stokes. As will be shown, the interaction between the sphere and the water is handled remarkably well by the solver using the general contact algorithm.

In order to ensure the fidelity of this model, specific attention is given to several aspects of the approach, which are described in detail in this paper. First, the constitutive model of the elastomer must incorporate large-strain behavior (i.e., hyperelastic model) and strain-rate effects (i.e., viscoelastic model). The choice of constitutive model and calibration of parameters from experimental testing is a key aspect of this study and is described in detail in Section 4. Section 6 presents further details of the numerical methods. In Section 7, numerical results are benchmarked against data analyzed from high-speed images of experiments. Validations are performed using and array of three angles of attack and three launch velocities that result in a representative range of sphere water impact physics.

The effect of friction at the solid-liquid interface is also considered in Section 8.1. The validity of the no-slip boundary condition is unclear for the sphere skipping phenomenon and therefore, frictionless vs. no-slip boundary conditions are both investigated to analyze the effect of friction on the behavior of the sphere and the fluid.

Finally, the mesh size is optimized to reduce the computational expense while maintaining sufficient accuracy. Being an explicit calculation, the solution time is dependent on the wave speed in the material and the finite element size. A brief mesh convergence study was presented at the SIMULIA East User's Conference (Jandron, 2013) and is further discussed in Section 8.2.

4. Physical Testing and Characterization of Elastomer

Filled silicone rubber exhibits highly non-linear mechanical behavior. This non-linearity is typically characterized by large strain levels under static conditions, a non-linear stress–strain response and strain-rate dependence. The strain-rate dependence usually relates to a stiffening of the material upon faster strain-rates.

Quasi-static (i.e. rate-independent) physical testing was performed using the Instron 5586 Testing Machine (Serial# H1503) with various goals in mind: (a) assess the material's response to large strains, (b) explore damage (e.g. permanent set and Mullin's effect) and hysteresis by cycling large strains, and (c) to determine ultimate tensile strength.

However, since the collision timescales are very short, we expect rate-dependent effects to be an important consideration as well. As such, viscoelastic properties are explored with stress-relaxation tests using a Dynastat Mark II Mechanical Spectrometer. The goals of the viscoelastic testing are to: (a) determine the frequency dependence of the material up to 1 kHz at room temperature, (b) identify the glass transition temperature of the material, T_g, and (c) explore the non-linear viscoelasticity effects by assessing dependence on strain amplitude.

4.1 Hyperelasticity

Hyperelastic effects need to be considered when the deformations are large because the elastomer undergoes different deformation mechanisms under load and may stiffen or soften as a function of strain. In the present study, strains on the order of 100% are common in the elastomer at impact.

For the hyperelastic constitutive model, the stress strain behavior is related by the strain energy (Bower, 2010). Various models exist, but one of the simplest is a neo-Hookean model. Since the elastomer is a cross-linked polymer and exhibits nearly incompressible behavior, we can use an incompressibility assumption to deduce an even simpler form of the strain energy potential. For an incompressible elastomer, the form of the neo-Hookean strain energy potential becomes

$$U = \frac{\mu_1}{2}(I_1 - 3), \tag{1}$$

where U is the strain energy per unit of reference volume, μ_1 is a material property (for small deformations, this can be regarded as the initial shear modulus of the solid), and I_1 is a deformation invariant. The incompressible Cauchy stress strain relationship follows as

$$\sigma_{ij} = \mu_1\left(B_{ij} - \frac{1}{3}B_{kk}\delta_{ij}\right) + \frac{p}{3}, \tag{2}$$

where B_{ij} is the left Cauchy Green deformation tensor, δ_{ij} is the Kronecker delta, and p is a term for hydrostatic stress which is solved for as part of the boundary value problem (BVP). Since the neo-Hookean model by definition cannot model the "upturn" in the stress strain response, the Ogden N=1 is also considered. The strain energy potential of the Ogden model is

$$U = \frac{2\mu_1}{\alpha^2}\left(\lambda_1^{\alpha_1} + \lambda_2^{\alpha_1} + \lambda_3^{\alpha_1} - 3\right) + \frac{p}{3}, \tag{3}$$

where μ_1 and α_1 are the two material parameters defining the hyperelastic model. The stress-strain relation is more complex than in the neo-Hookean case, and will not be written out here.

The constitutive models were calibrated using a quasi-static uniaxial Instron test. The tension specimen was cut into a small ASTM dogbone shape. The dogbone was stretched to more than 600% and a least squares approach was used to determine the material parameters to the neo-Hookean and Odgen models.

The neo-Hookean model requires one parameter to be calibrated, while the Odgen N=1 model requires two parameters. In this case, Equation 2 can be solved for the uniaxial tension boundary conditions assuming volume preserving uniaxial stretch to conclude the following relation, in terms of nominal stress

$$S_1 = \mu_1(\lambda - \lambda^{-2}), \tag{4}$$

where S_1 is the nominal stress, λ is the stretch, and μ_1 is the unknown parameter. Nominal stress and stretch are measured in a uniaxial tension test and thus μ_1 can be fit by minimizing the difference between predicted and measured S_1 values in a least-squares sense. This can be solved in MATLAB or Abaqus/CAE using the material evaluation tool. Similarly, for the Ogden N=1 model, Equation 3 becomes

$$S_1 = \frac{\mu_1}{\lambda}\left(\lambda^{\alpha_1} - \lambda^{-\alpha_1/2}\right), \tag{5}$$

where and additional parameter α_1 must also be estimated. This is a non-linear least squares problem, but still solvable using Matlab or Abaqus/CAE. For the current study, Equations 4 and 5 are solved using MATLAB and computed fits are shown in Figure 1 with the Instron data superimposed. It is clear that the neo-Hookean is not suitable above 100% strain because it cannot capture the "upturn" in the response, while the Odgen N=1 model captures the response accurately up to failure. Table 2 shows the final material parameters for the Dragon-Skin silicone material used in the analysis.

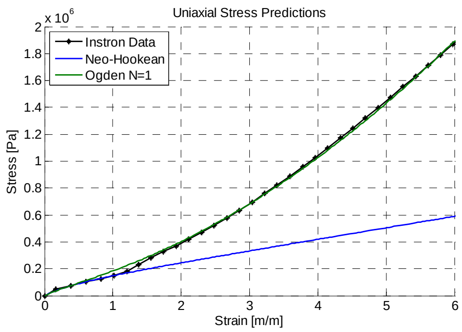

(a)

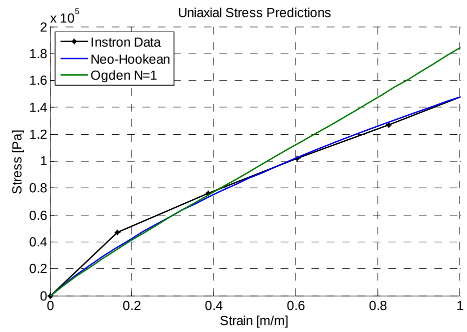

(b)

Figure 2. (a) Quality of neo-Hookean and Ogden *N*=1 fit up to 600% strain; (b) Quality of fit under 100% strain. Note that the neo-Hookean is very accurate below 100% strain.

Table 2. Hyperelastic model parameters.

Model	μ_1 [Pa]	α_1	Valid Range
neo-Hookean	89,170	N/A	< 100% Strain
Ogden N=1	55,307	2.8156	< 600% Strain

For the present study, the neo-Hookean is used since deformations are less than 100% strain for all considered cases. It is expected that higher speed impacts and more compliant materials will facilitate the need to models other than the neo-Hookean. However, this purely elastic model cannot represent the strain-rate stiffening that is observed from the high velocity impacts in the elastomer. This indicates a need to characterize the viscoelastic aspects of the material and is further explained in Section 4.2.

4.2 Viscoelasticity

Viscoelasticity is the study of materials exhibiting of both elastic and viscous behavior (Ferry, 1970) and is an important consideration in materials that are used at temperatures near or above their glass transition temperature, T_g. A viscoelastic model is characterized by a rate-independent (or long-term) shear modulus, G_∞, which is indicative of a purely elastic model (e.g. the neo-Hookean hyperelastic model), and a rate-dependent shear modulus defined by a Prony Series (Bower, 2010). Note here that $G_\infty = \mu_1$ for the neo-Hookean and Odgen model since they were calibrated with quasi-static, or long-term uniaxial testing. The Prony Series is a means to compute an instantaneous modulus in the material based on time. In other words, faster strain-rates will induce a higher instantaneous modulus than a quasi-static loading. In a linear viscoelastic model, the instantaneous modulus, $G(t)$, is defined as

$$G(t) = G_\infty + \sum_{i=1}^{N} G_i e^{-t/\tau_i}, \tag{6}$$

where G_∞ is the infinite shear modulus, defined from the quasi-static hyperelasticity model, and G_i, τ_i, i = 1..*N* are the moduli and time constants of the Prony Series, respectively. Graphically, a linear viscoelastic model of *N*=3 can be interpreted as a set of three Maxwell elements in parallel describing the Prony Series with an elastic modulus describing the elastic modulus in parallel. This is shown in Figure 3.

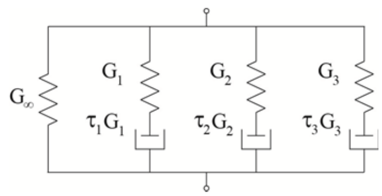

Figure 3. Three term Prony series interpretation. G_∞ represents the long-term elastic modulus in parallel with three Maxwell elements defining the viscoelastic model.

Calibration of the Prony series requires determining the G_i and τ_i coefficients for the silicone from experimental data A stress relaxation test was performed at room temperature using the Dynastat testing machine. A strain of 10% uniaxial compression was prescribed within 1.01E-02 seconds and held adiabatically for 1.00E+03 seconds. Mechanical limitations prevented quicker loading rates, so the maximum strain-rate content in the data is 1/1.01E-02 seconds, or 9.87E+01 Hz. Given the force and displacement data verses time, it is straightforward to compute the nominal stress and strain in the specimen. From this, the tensile elastic modulus is determined versus time, and the shear modulus versus time follows from the incompressibility assumption (i.e. the uniaxial modulus is approximately three times the shear modulus). The experimental shear relaxation modulus, *G(t),* is normalized with respect to the peak modulus, G_0, in order to enter the data into Abaqus using *g(t)*. Figure 4(a) shows the normalized shear modulus data in addition to the best fit to a *N*=3 Prony series determined by Abaqus/CAE using the material evaluation tool.

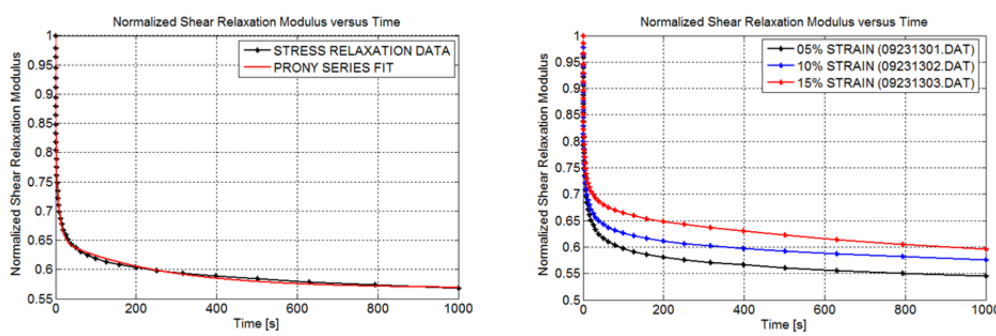

(a) (b)

Figure 4. (a) Stress relaxation data and Prony Series fit used in model. The initial strain corresponds to 10% strain; (b) Strain amplitude dependence on relaxation modulus showing non-linear viscoelastic effects. It shows the material is stiffer when stretched to higher initial strains during the stress relaxation experiment.

It is good practice to match the maximum order of the Prony Series fit with the number of decades of time data in the experiment. In this case, Abaqus/CAE determined the best fit to be N=3 which corresponds with three decades of time in the 1.00E+03 second experiment. Table 3 gives the coefficients for the best fit computed by Abaqus/CAE.

Table 3. Prony series coefficients.

g_1	τ_1 [s]	g_2	τ_2 [s]	g_3	τ_3 [s]
1.9605E-01	6.6032E-01	1.5283E-01	9.3863E+00	8.3333E-02	2.5137E+02

Linear viscoelasticity does not provide a means to model a dependence on strain amplitude. Consider a stress relaxation test where a specimen is initially strained to 5% strain and held for a long time. Then the specimen is unloaded for a long time and the process is repeated for 10% initial strain. Finally the process is repeated a third time for 15% initial strain. Normalizing the moduli in all three cases will yield an identical response in a linear viscoelastic material. A non-linear viscoelastic material includes the ability to model the dependence on strain amplitude. Preliminary tests indicate the silicone shows non-linear viscoelastic effects, as shown in Figure 4(b). This effect is neglected for the time being for simplicity, but may be an important consideration for future study; particularly for more compliant materials and higher speed impacts.

While it is also possible to conduct a separate experiment on the volumetric response of the silicone (i.e. determine a separate Prony Series for volumetric behavior), this is ignored for the present study under the assumption of incompressibility. Additionally, a preliminary repeatability study was considered by performing a stress relaxation test on two separate days with the same specimen subject to approximately the same test conditions. A maximum difference of 1.5% was found over the 1.00E+03 second test, and thus deemed repeatable.

4.3 Complete Constitutive Model

The solid is governed by the conservation of momentum,

$$\rho\ddot{\mathbf{u}} - \nabla\cdot\boldsymbol{\sigma} = \rho\mathbf{b}, \tag{7}$$

where ρ is the material density, $\ddot{\mathbf{u}}$ is the acceleration, **b** are the body forces, and the Cauchy stress tensor, $\boldsymbol{\sigma}$, is computed with the constitutive model using the neo-Hookean hyperelasticity model and the N=3 Prony Series linear viscoelastic model.

The final material properties describing the constitutive model in Abaqus/Explicit are shown in Table 4. Note that the hyperelastic parameters have been written in a format compatible with Abaqus.

Table 4. Final elastomer material properties defined in Abaqus/Explicit.

Density	Hyperelasticity (neo-Hookean)		Viscoelasticity (Time-Domain Linear Viscoelasticity)			
P [kg/m^3]	C_{10} [Pa]	4.459E+04	g_1	1.9605E-01	τ_1 [s]	6.6032E-01
1.050E+03	D_1 [Pa]	0	g_2	1.5283E-01	τ_2 [s]	9.3863E+00
			g_3	8.3333E-02	τ_3 [s]	2.5137E+02

It is worth noting that by default Abaqus/Explicit must assume some compressibility in the material model to compute a reasonable wave speed. Hence, the value describing the bulk modulus, D_1, in Table 5, is ignored and a default value implying a Poisson's ratio of $\nu = 0.475$ is used instead (Abaqus, 2013). The effect of this compressibility on the current model has not yet been studied.

5. Fluid Properties

The fluid is governed by the general Navier-Stokes equation without bulk viscosity (Abaqus, 2014),

$$\rho \frac{D\boldsymbol{v}}{Dt} = -\nabla \mathrm{p} + \eta \nabla^2 \boldsymbol{v} + \frac{\boldsymbol{\eta}}{\mathbf{3}} \nabla(\nabla \cdot \boldsymbol{v}) + \rho \boldsymbol{b}, \qquad \textbf{(8)}$$

where η is the viscosity, ρ is the density, p is the pressure, *v* is the velocity, and **b** represents body forces. Note that bulk viscosity has been set to zero in the Abaqus/Explicit dynamic step to assume Equation 8. The relationship between density and pressure is governed by a Equation of State (EOS) model. A linear U_s-U_p Hugoniot form of the Mie-Gruneisen EOS is used to evaluate the pressure in the water in the simulation. Using this implementation, the water is modeled as a compressible viscous fluid. The constitutive model takes the form

$$\mathrm{p} = \frac{\rho_0 c_0^2 \eta}{(1 - s\eta)^2}\left(1 - \frac{\Gamma_0 \eta}{2}\right) + \Gamma_0 \rho_0 E_m, \qquad (9)$$

where p is the pressure, ρ_0 is the reference density, α is the nominal volumetric compressive strain, E_m is the specific energy, Γ_0 is the Gruneisen ratio, and c_0 and s are defined by a linear relation between the shock velocity, U_s, and the particle velocity, U_p, such that,

$$U_s = c_0 + sU_p. \qquad (10)$$

The appropriate parameters chosen to represent water are tabulated in Table 5 and reduce Equation 9 to

$$\mathrm{p} = K_0 \alpha, \qquad (11)$$

where the (small strain) bulk modulus is defined by $K = \rho_0 c_0^2$, which is approximately K = 2.2E+09 Pa, and $\alpha = (1 - \rho_0/\rho)$ is the nominal volumetric compressive strain. An incompressibility assumption is not feasible in Abaqus/Explicit because it implies an infinite wave speed which cannot be handled with explicit time integration methods. These parameters are representative of water, but a rigorous study into a more appropriate model has not been performed. Also note that cavitation effects need not be considered here and that the expected rate of deformation is orders of magnitude less than the fluid wave speed.

Table 5. Final fluid properties defined in Abaqus/Explicit.

Linear Us-Up Model			Density	Viscosity
C_0 [m/s]	S	Γ_0	ρ [kg/m³]	ν [Pa-s]
1.483E+03	0	0	1.000E+03	8.9E-04

6. Skipping Sphere Model

The model consists of two parts: the water tank and the elastomeric sphere and is modeled in a 3D space. A half symmetry is also assumed in the model to consider the trajectory in the Z = 0 plane only. The tank is chosen as small as possible while ensuring edge effects are minimized. A 2D view of the model is shown in Figure 5 – note this is a 2D view of a 3D model. Initially void regions are highlighted. SI units are adopted universally for this effort, with dimensions in meters. The sphere has a radius of 2.54E-02 meters (1 inch) for all cases presented in this paper. The fluid domain is 8.00E-01 meters in length, 1.00E-01 meters in width, and 2.50E-01 meters in height.

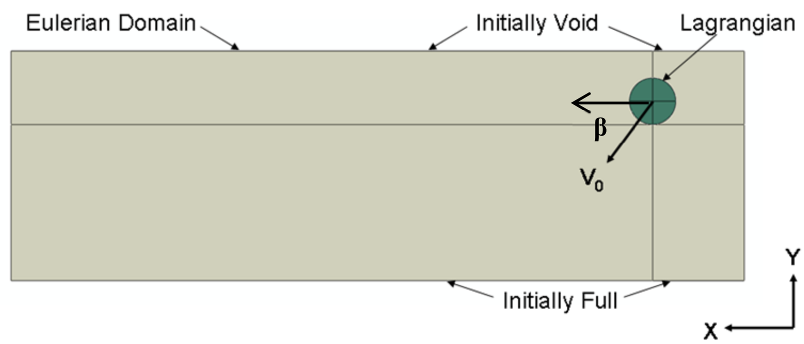

Figure 5. Model idealization in Abaqus/CAE.

Interaction between the water and the sphere is handled with general contact in Abaqus/Explicit using a frictionless contact property for tangential behavior and a hard contact pressure-overclosure property for the normal behavior. A nominal mesh density of 6.00E-03 meters is used for both the sphere and fluid domain since this is preferable for the contact algorithm. The mesh consists of 93,398 linear 8-noded Eulerian hexahedral elements to represent the water and 276 linear 8-noded (Lagrangian) hexahedral elements to represent the sphere. Section 8.2 considers the effects of mesh size on solution accuracy.

An Abaqus/Explicit solution procedure is used with a total step time of 1.00E-01 seconds. This is shown to be a sufficient amount of time for most cases to either completely skip or become entrained in the fluid. As discussed in Section 5, a solution parameter, bulk viscosity, has also been set to zero for this step to minimize artificial energy dissipation.

Symmetry boundary conditions are applied in the plane of symmetry in the Initial step, and Eulerian boundaries are applied in the dynamic explicit step. The Eulerian boundaries include: No Inflow with Nonreflecting Outflow on the bottom surface of the tank, and Free Inflow with Nonreflecting Outflow on all remaining sides of the tank. The top surface is unconstrained. The intent of these boundary conditions is to represent a large infinite tank where material can freely flow through the boundary of the mesh. Note that the effect of atmospheric pressure is not included in this analysis.

An initial velocity, V_0, is prescribed on the sphere just before impact using a predefined field. The velocity vector makes an angle with the horizontal defined as $\beta = \tan^{-1}(V_y / V_x)$. The velocity is determined from the high-speed cameras, which includes a ±3% uncertainty. Table 7 summarizes these velocities for the range of test cases considered in this paper. In addition, a gravity body force of 9.81E+00 is applied to the entire model in the negative Y direction.

Table 7. Prescribed initial velocity, V_0.

	β = 20º	β = 30º	β = 40º
V_L **(m/s)**	1.683E+01	1.270E+01	1.428E+01
V_M **(m/s)**	2.070E+01	2.070E+01	1.620E+01
V_H **(m/s)**	2.820E+01	3.890E+01	3.570E+01

7. Analysis Results

The simulations are completed using Abaqus/Explicit 6.13-1 on a Windows 7 desktop using 8 cores. The analysis solved for 100 ms of results which completed in approximately 50 minutes of runtime. A snap shot of all cases at 10 ms is shown in Figure 6. Excellent qualitative agreement is observed in both the response of the sphere and also the size and shape of the fluid cavity. Note that all cases along the diagonal are in a transitional phase (where the sphere travels horizontal just below the water surface), all cases below the diagonal fail to skip, while all cases above the diagonal successfully skip. In all cases the Abaqus simulation is able to accurately predict skipping.

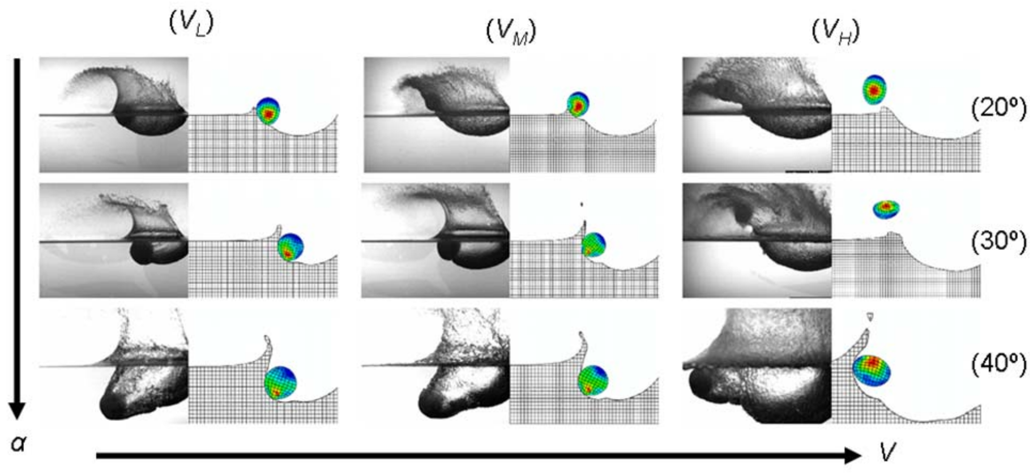

Figure 6. Snapshot comparison of all cases at 10 ms

A time series plot is shown in Figure 7 for the low speed, β = 20º case. The analysis shows rich features of the fluid-structure interaction. A shear wave is initiated upon impact with the free-surface of the water at 2.5 ms, and propagates clockwise around the periphery of the sphere (2.5 – 7.5 ms). The shear wave impacts the water cavity between 7.5 ms and 10 ms and again just before 20 ms; this impact transmits energy from the sphere to the water. These impacts cause the cavity to change shape, which is observed in both the analysis and the experiment.

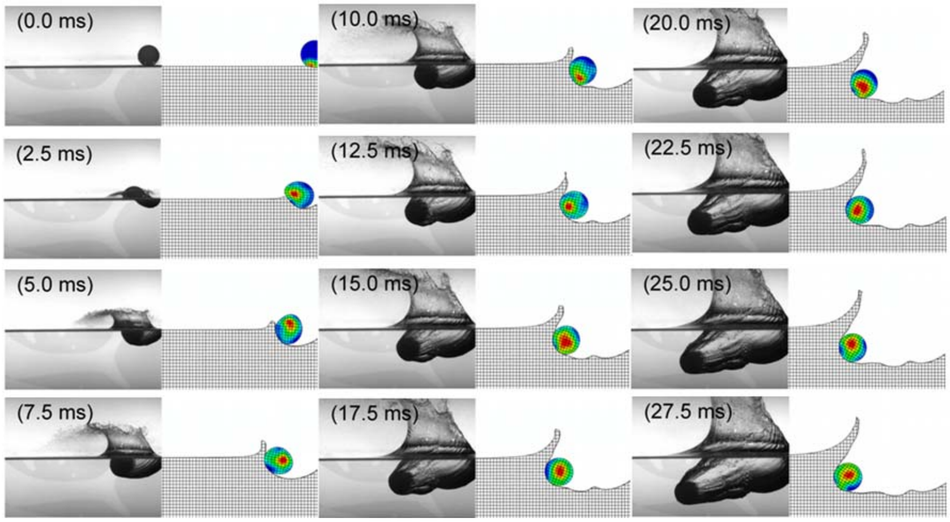

Figure 7. Waterfall comparison for low speed, α = 20º case.

To optimize the skipping mechanism of the sphere it is desirable to conserve total energy in the sphere. This can be assessed by inspecting the strain energy and kinetic energy in the sphere versus time. By normalizing the strain energy with the initial kinetic energy in the analysis, a dimensionless energy ratio can be determined. This energy ratio is shown in Figure 8(a). Interestingly, upon comparison to Figure 6, a correspondence between successful skipping and high energy ratios can be made.

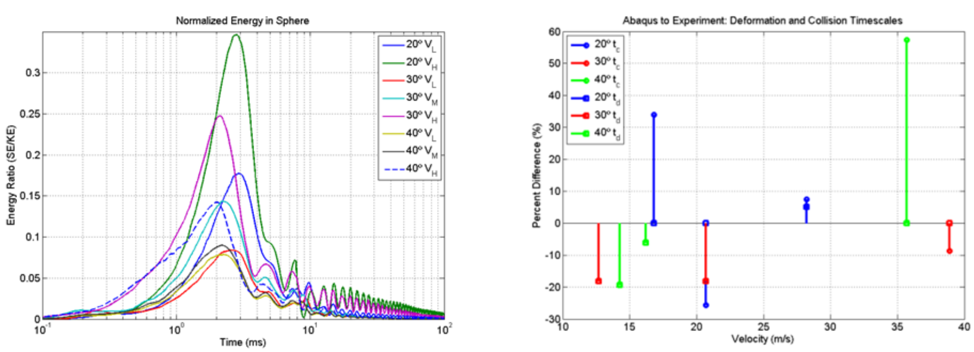

Figure 8. (a) Normalized energy (total strain energy/initial kinetic energy); (b) Percent error of collision and deformation times from Abaqus relative to experiment.

Lastly, the deformation time and collision time is considered. As mentioned in Section 1, the collision time, t_c, is the total time the sphere is in contact with the water, and the deformation time,

t_d, is the time for an elastic wave to propagate through the elastomer and impact the fluid cavity wall. It is observed from experiments that the likelihood of skipping is increased when $t_c < t_d$. Therefore t_c and t_d are important parameters to deduce from the Abaqus simulation. Figure 8(b) shows the percent difference between the Abaqus simulation and the measured experiment. From Figure 8(b), t_d agrees within ±20% and t_c agrees within ±60%. The significance is that Abaqus is able to predict the deformation time of the ball well within a range of strain-rates. The collision time is difficult to compare because flow is not as resolved in the simulation. A more refined fluid mesh is expected to reduce this difference further.

8. Supplemental Investigations

8.1 Effect of Friction

The effect of a no-slip, i.e. rough friction, implementation in the contact interaction is explored in comparison with a frictionless implementation. The case shown in Figure 8 is for low speed, β = 30º impact. It is clear the rough friction model is inappropriate for use in the model because the cavity formation is not physical and the friction also seems to erroneously affect the trajectory of the sphere. By contrast, the frictionless model is able to capture the cavity shape and sphere trajectory very well.

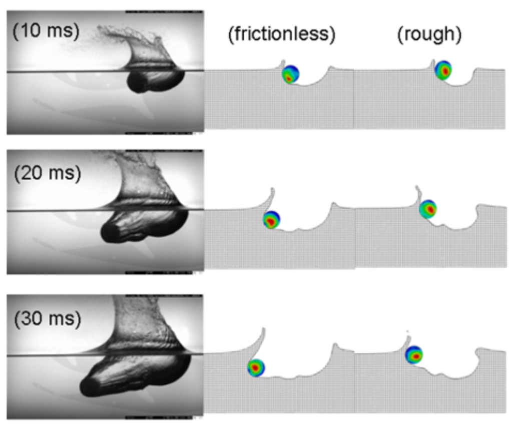

Figure 8. Friction comparison of low speed, β = 30º at 10 ms

8.2 Effect of Mesh Density

In order to qualitatively assess agreement with experiment, a simple mesh density study is performed. In this case, both the mesh of the sphere and the fluid domain are varied with 3 mm, 6 mm, 12 mm, and 24 mm mesh densities. The results are shown in Figure 8 for one case of β and V_0. The relative computational expense ratio for these cases is: 1.0E+00, 1.1E-01, 1.6E-02, 3.7E-03, respectively. The results are shown in Figure 8 which indicates the 3 mm case is the most accurate; the 6 mm case shows a slight error in the trajectory angle, and the 12 mm and 24 mm meshes give incorrect solutions – they show the sphere erroneously skipping.

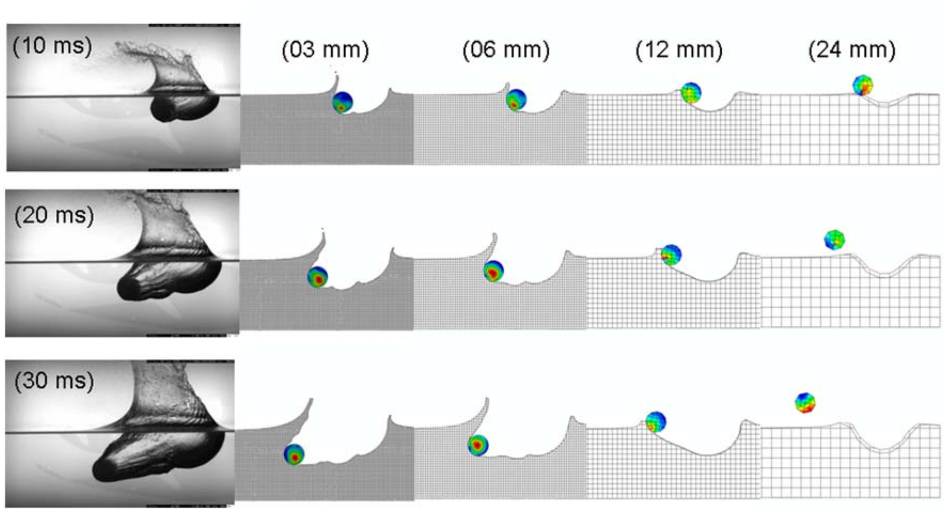

Figure 8. Mesh density comparison for the low speed, β = 30º case at 10 ms

As a result, the nominal case used in the present paper is 6 mm because it offers reasonable accuracy and solves nine times quicker than the 3 mm case. However, 3 mm meshes will be considered for future work when the analysis is performed on the NUWC supercomputing cluster. A mesh convergence study with mesh densities finer than 3 mm will be considered in the future.

9. Conclusions

This paper shows that a sphere modeled with a simple neo-Hookean hyperelastic and a linear viscoelasticity constitutive model gives qualitatively and quantitatively accurate solutions using Abaqus/Explicit. In all cases, the Abaqus/Explicit model is able to predict the skipping phenomenon of the spheres with comparison to high-speed images. It was found that the mesh density strongly affects the fluid-structure interaction of the sphere with the water and that a convergence study should be performed in future studies involving CEL. However, this can very computationally expensive, so adaptive meshing schemes may be attractive. It was also found that a frictionless contact definition is most physical to represent a silicone sphere in contact with water. The model presented in this paper will be useful to perform parametric studies regarding the design of optimal skipping objects and future work will exploit this capability. For example, more compliant spheres, hollow spheres, and spheres with inclusions can be studied with the end goal of designing an optimal skipping object.

Future improvements to the model will be focused on obtaining stress relaxation data at higher strain-rates, further investigating the non-linear viscoelastic effects, and an investigation into the effectiveness of the current viscoelastic model to predict losses in the material (Dalrymple, 2007). If insufficient, a frequency-domain Dynamic Mechanical Analysis (DMA) test may be considered in order to quantify the storage and loss moduli of the material (Sternstein, 1983). In addition, a range of elastomers will be tested to further assess the validity of the model.

In addition, future analysis and experiments are planned to explore the fluid-structure interaction of spheres performing multiple skips. This will pose unique computational challenges because the duration and the number of finite elements in the simulation will likely increase.

10. References

1. Abaqus Documentation, Ver. 6.13-1, Dassault Systémes SIMULIA Corp., Providence, RI.
2. Abaqus Knowledge Base, "Effective Fluid Equations Used in Coupled Eulerian-Lagrangian (CEL) Analyses," QA Article: QA00000008508, Jan. 14, 2014.
3. Belden, J., Jandron, M. A., Truscott, T.T., "Physics of Elastic Spheres Skipping on Water." Proceedings, Physics of Sports. Ecole Polytechnique, Paris, France. April 3-6, 2012.
4. Bower, A. F., "Applied Mechanics of Solids," CRC Press, 2010.
5. Clanet, C., Hersen, F., Bocquet, L., "Secrets of Successful Stone-Skipping," Nature **427**, 29 (2004).
6. Dalrymple, T., Choi, J., and Miller, K., "Elastomer Rate-Dependence: A Testing and Material Modeling Methodology," Proceedings, Fall 172nd Technical Meeting of the Rubber Division of the American Chemical Society, Inc., Cleveland, OH, 2007.
7. Ferry, J. D. "Viscoelastic Properties of Polymers," Wiley, New York, 1970
8. Jandron, M., Belden J., Fennell, W., "Modeling of Hyperelastic Skipping Spheres using Abaqus/Explicit, Presentation," SIMULIA East Regional User Meeting, Providence, RI, September 18, 2013
9. W. Johnson, S.R. Reid, ARCHIVE: Journal of Mechanical Engineering Science 1959-1982 (vols 1-23) 17(2), 71 (1975).
10. G.V. Logvinovich, "Hydrodynamics of Free-Boundary Flows," Tech. rep., Jerusalem, Israel Program for Scientific Translation, (1972).
11. MATLAB, R2010b, The MathWorks Inc., Natick, MA, 2010.
12. May, A., "Water Entry and the Cavity-Running Behavior of Missiles," Tech. rep., NAVSEA Hydroballistics Advisory Committee, Silver Spring, MD, 1975.
13. Miloh, T., "On the Oblique Water-Entry Problem of a Rigid Sphere," Journal of Engineering Mathematics 25, 77 (1991).
14. Rosellini, L., Hersen, F., Clanet, C., Bocquet, L., "Skipping Stones," Journal of Fluid Mechanics **543**, 137 (2005).
15. Sternstein, S. S., "Transient and Dynamic Characterization of Viscoelastic Solids," American Chemical Society, 1983.
16. Truscott, T.T., Beal, D.N., Techet, A.H., in Proceedings of the 7th International Symposium on Cavitation, Ann Arbor, Michigan, USA, 2009.

11. Acknowledgements

This project is supported in part by the NUWC Section 219 Basic Research program monitored by Neil DuBois, and in part by the University Laboratory Initiative (ULI) at the Office of Naval Research (ONR). Sponsor support is gratefully acknowledged.